Supporting Information

Slow Magnetic Relaxation in Neutral *0D* and *1D* Assemblies of a Mn(III) Schiff Base Complex and Heptacyanorhenate(IV)

Taisiya S. Sukhikh [1], Wernsdorfer Wolfgang [2], and Kira E. Vostrikova [1,*]

[1] Nikolaev Institute of Inorganic Chemistry SB RAS, 3 Lavrentiev Avenue, 630090 Novosibirsk, Russia;
[2] Physikalisches Institut, Karlsruhe Institute of Technology, 1 Wolfgang-Gaede-Str., D-76131 Karlsruhe,

Table S1. SCXRD Experimental details

	1	**2**
Chemical formula	$C_{31}H_{34}MnN_{11}O_2Re\cdot 7H_2O$	$C_{31}H_{34}MnN_{11}O_2Re\cdot 3H_2O$
M_w	959.93	887.88
Crystal system, space group	Monoclinic, $P2_1/c$	Monoclinic, $P2_1/n$
Temperature (K)	150	150
a, b, c (Å)	11.5292 (11) 17.9419 (14) 19.0885 (17)	12.3733(6) 22.9922 (11) 12.7619 (6)
α, β, γ (°)	90 95.031 (3) 90	90 93.070 (2) 90
V (Å^3)	3933.4 (6)	3625.4 (3)
Z	4	4
Radiation type	Mo $K\alpha$, λ = 0.71073	Mo $K\alpha$, λ = 0.71073
μ (mm^{-1})	3.46	3.74
Crystal size (mm)	0.18 × 0.13 × 0.1	0.28 × 0.15 × 0.11
Diffractometer	Bruker Apex DUO	
T_{min}, T_{max}	0.607, 0.745	0.596, 0.745
Nº of measured, independent observed [$I>2\sigma(I)$] reflections	43075, 7545, 5967	53843, 6903, 6392
R_{int}	0.028	0.019
q values (°)	θ_{max} = 25.8, θ_{min} = 1.6	θ_{max} = 25.7, θ_{min} = 2.4
Range of h, k, l	-14 ≤ h ≤ 14 -21 ≤ k ≤ 21 -23 ≤ l ≤ 23	-15 ≤ h ≤ 15 -28 ≤ k ≤ 28 -15 ≤ l ≤ 15
$R[F^2 > 2\sigma(F^2)]$, $wR(F^2)$, S	0.040, 0.111, 1.07	0.040, 0.111, 1.07
No. of reflections, parameters, restraints	7545, 484, 0	6903, 455, 1
H-atom treatment	H-atom parameters constrained	H-atom parameters constrained
Weighting scheme	$w=1/[\sigma^2(F_o^2)+(0.049P)^2+19.910P]$ where $P = (F_o^2 + 2F_c^2)/3$	$w=1/[\sigma^2(F_o^2)+(0.015P)^2+5.297P]$ where $P=(F_o^2+2F_c^2)/3$
$\Delta\rho_{max}$, $\Delta\rho_{min}$ (e Å^{-3})	3.88, -0.71	0.86, -0.53

Absorption corrections were applied with the use of the SADABS program [APEX2 (Version 2.0), SAINT (Version 8.18c), and SADABS (Version 2.11), Bruker Advanced X-ray Solutions, Bruker AXS Inc., Madison, Wisconsin, USA, 2000–2012.]. The crystal structure was solved by direct methods and refined by full-matrix least squares techniques with the use of the SHELXTL package [Sheldrick, G.M. (2015). Acta Cryst. C71, 3-8]. Computer programs: *APEX3* (Bruker-AXS, 2016), *SAINT* (Bruker-AXS, 2016), *SHELXT* 2014/5 (Sheldrick, 2014), *SHELXL2017*/1 (Sheldrick, 2017). Atomic thermal displacement parameters for non-hydrogen atoms were refined anisotropically. The positions of hydrogen atoms were calculated corresponding to their geometrical conditions and refined using the riding model.

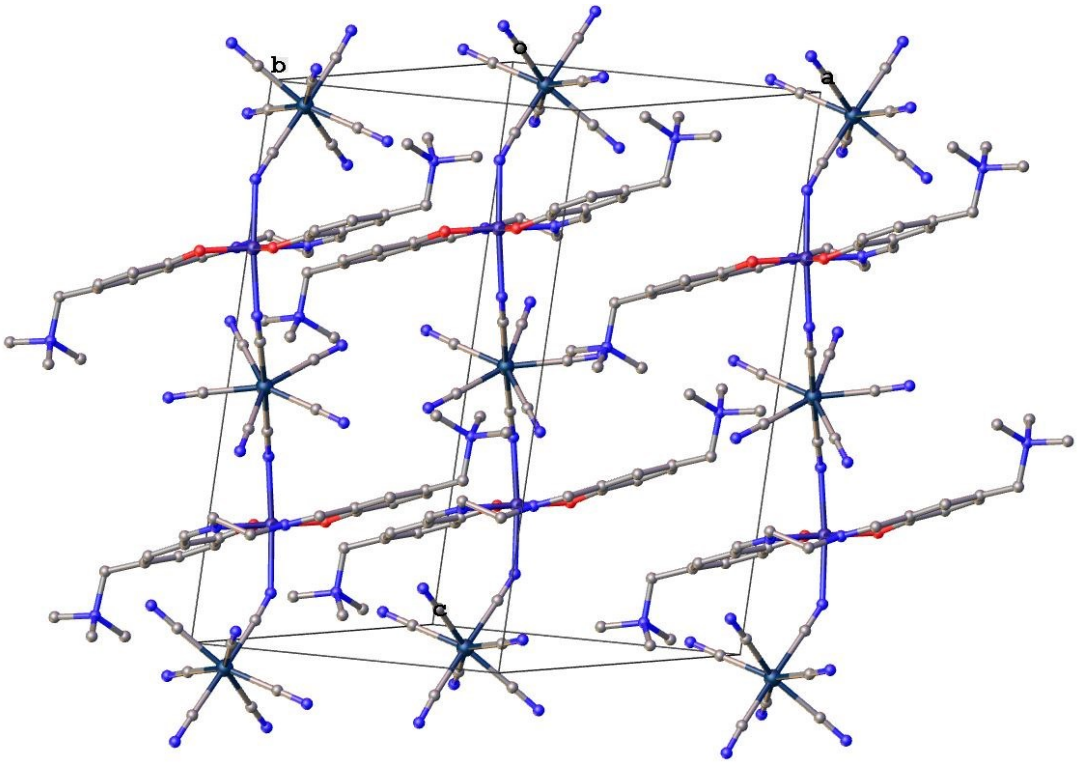

Figure S1. A view of chains packing in a crystal of **1** demonstrating a trans-location of the $[Me_3N^+CH_2]$ substituents relatively to a SB^{2+} plane. Hydrogen atoms are omitted for clarity.

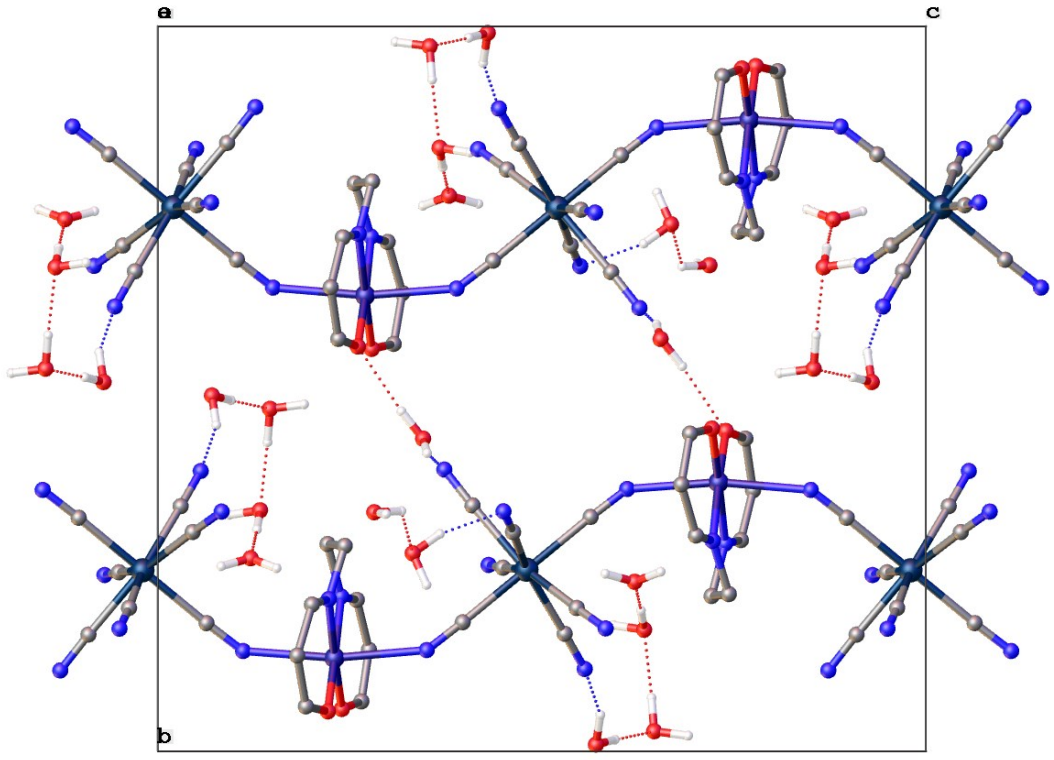

Figure S2. A layer formation in a crystal of **1**: H_2O molecules bind the fragments $[Mn^{III}(SB^{2+})]^{3+}$ and $[Re(CN)_7]^{3-}$ belonging to the different chains. The layers are interconnecting by means of interstitial water molecules. The SB^{2+}-ligands are reduced for clarity.

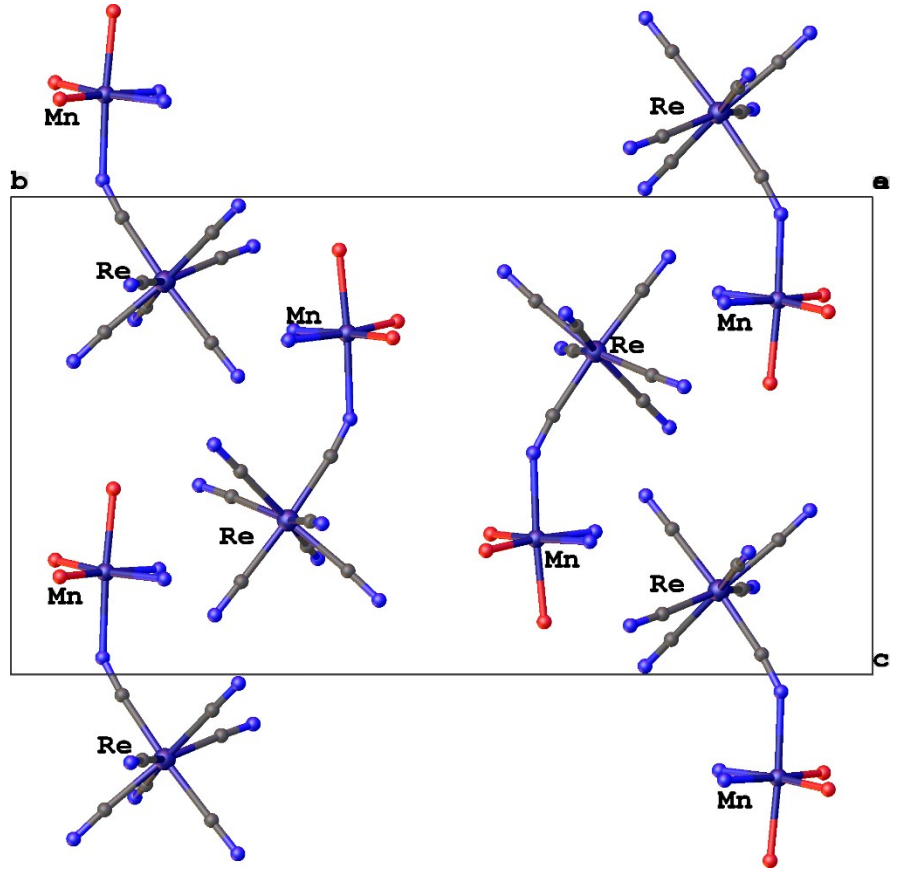

Figure S3. A view of dimers packing in a crystal of **2**. The SB^{2+}-ligands are reduced, and hydrogen atoms are omitted for clarity.

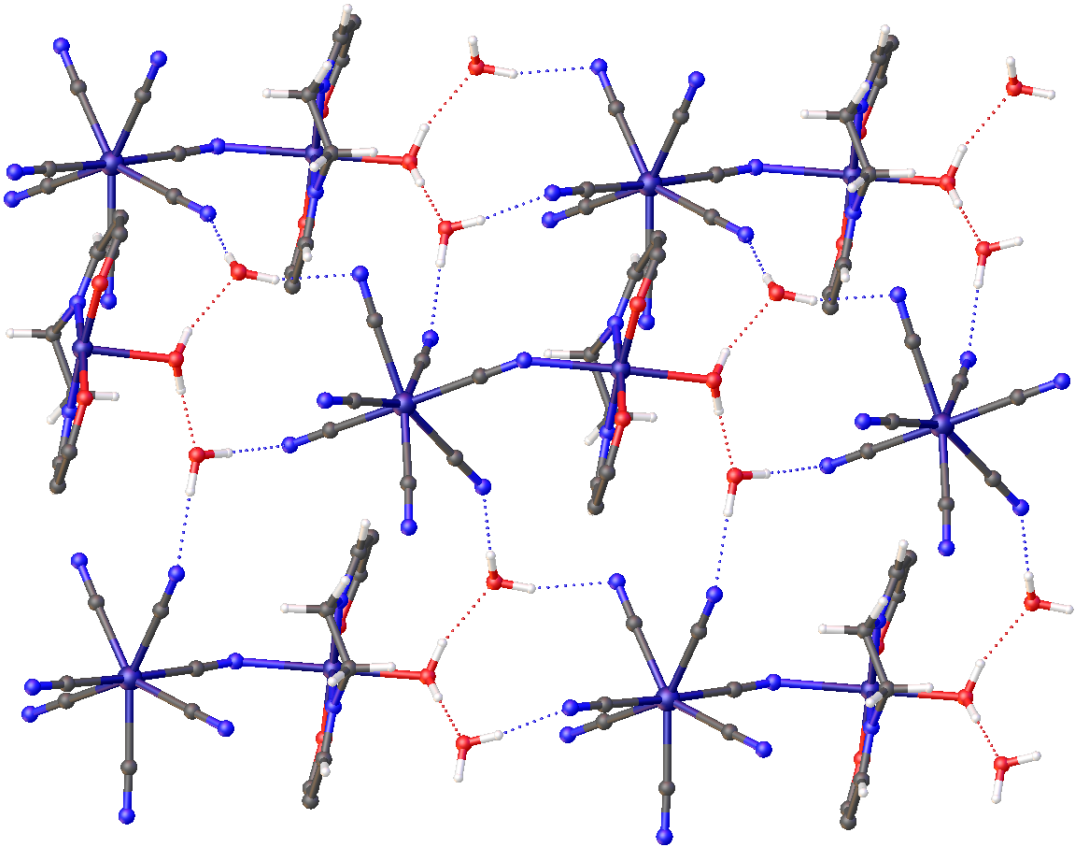

Figure S4. A layer formation in a crystal of **2**: H_2O molecules bind the fragments $[Mn^{III}(SB^{2+})]^{3+}$ and $[Re(CN)_7]^{3-}$ belonging to the different chains. The layers are interconnecting by means of interstitial water molecules. The hydrogen atoms are partially omitted for clarity.

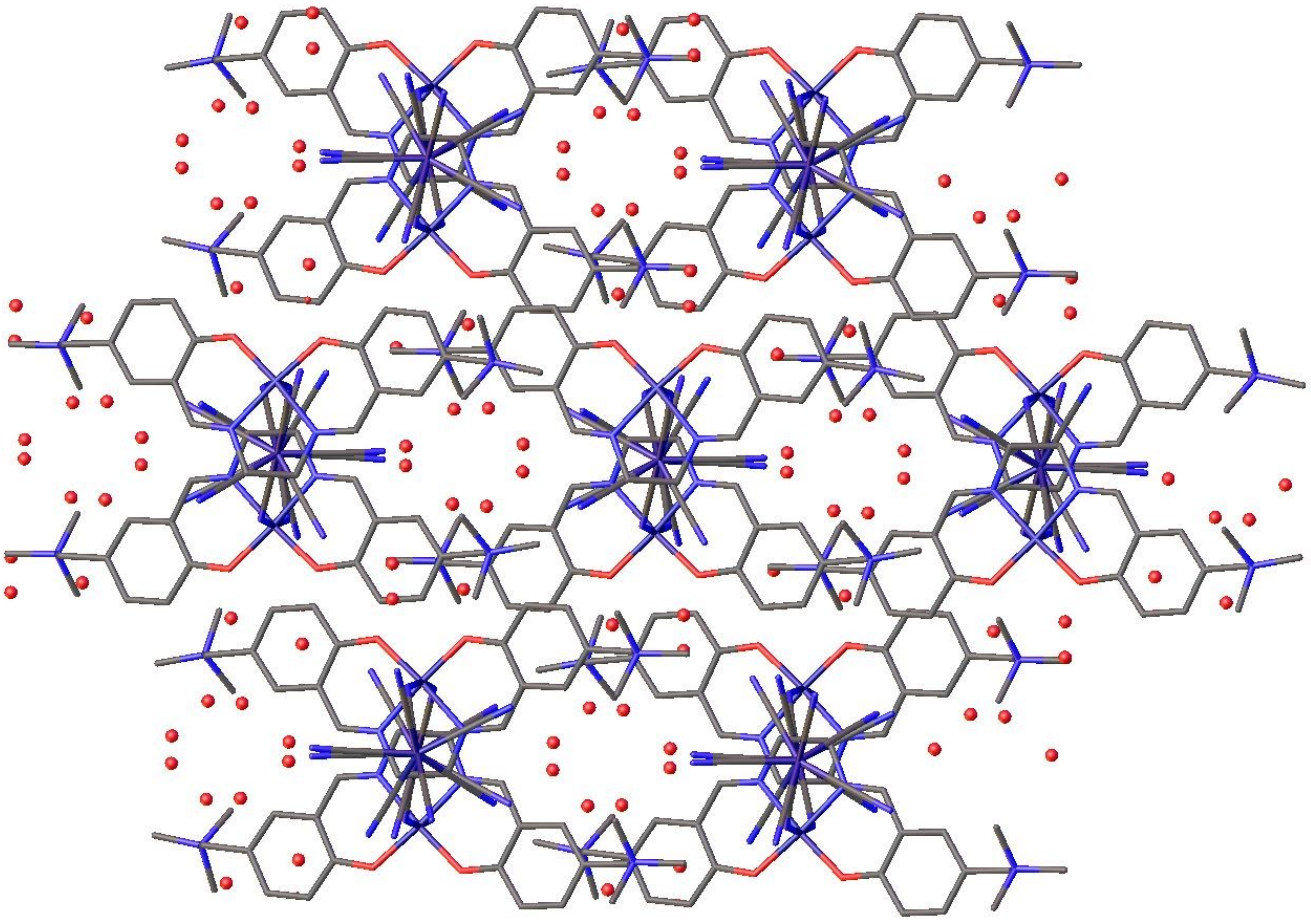

(a)

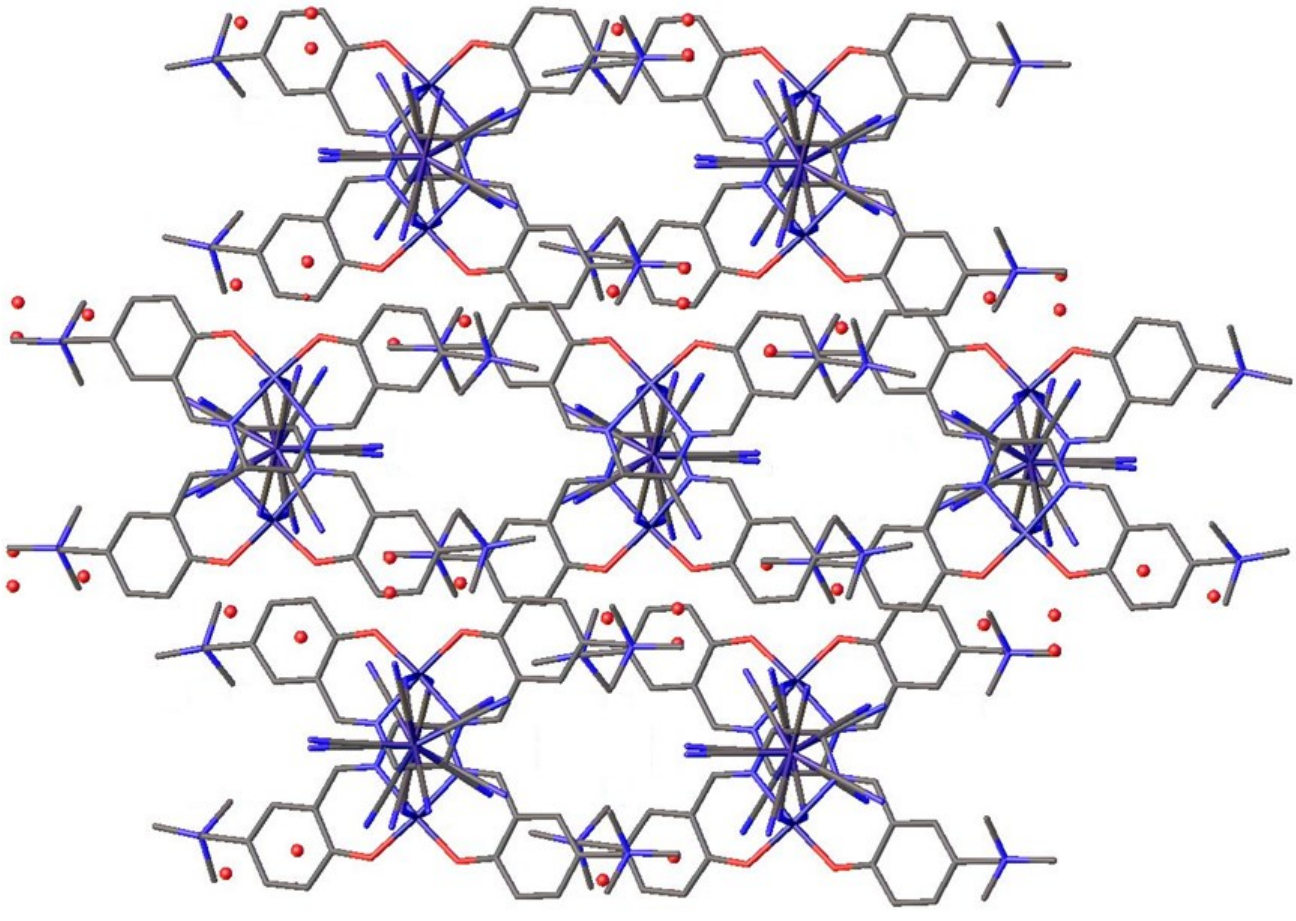

(b)

Figure S5. A view (in c-axis direction) of channels in a crystal of **1**: (a) filled by water molecules, (b) empty.

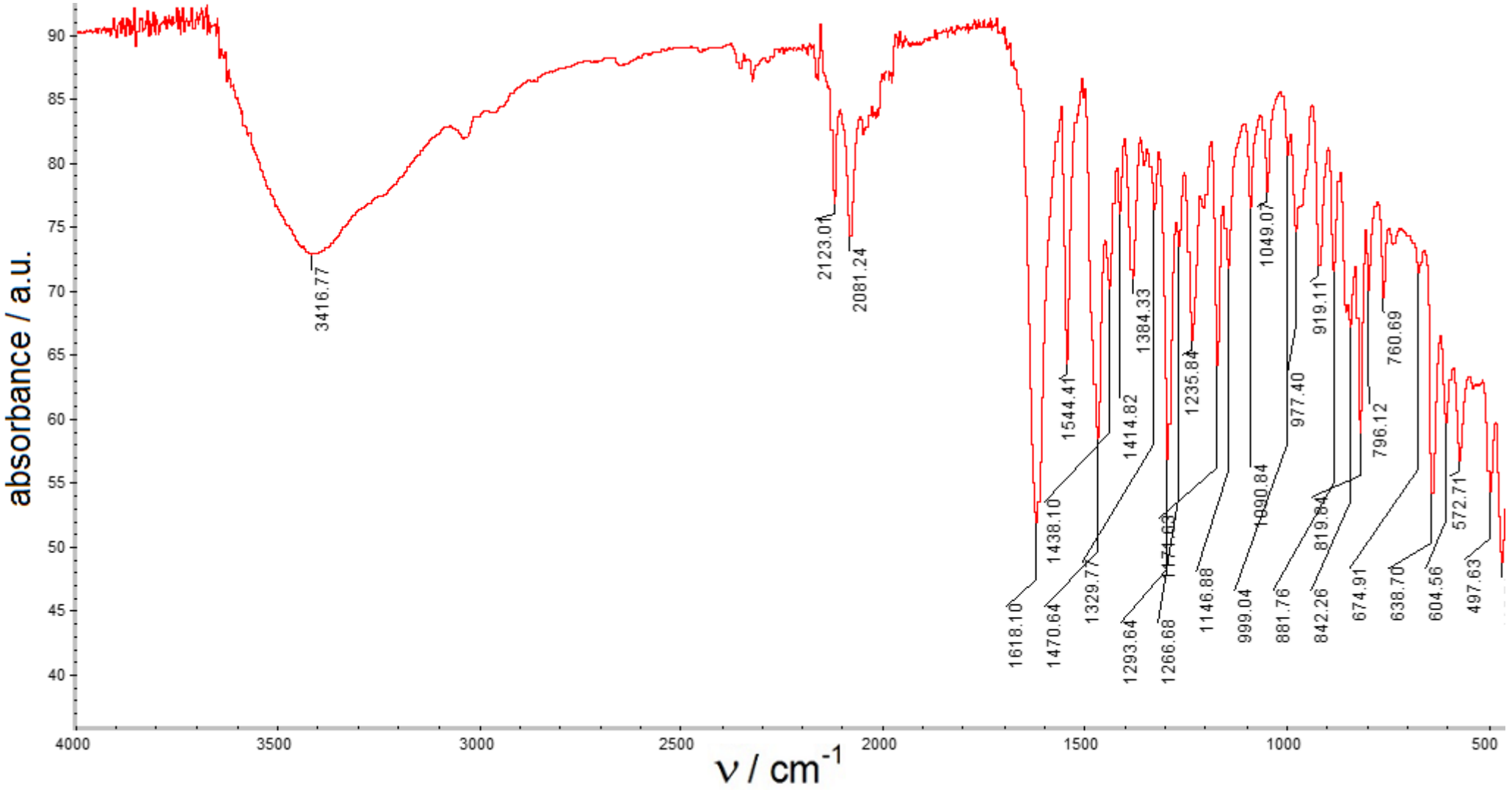

Figure S6. ATR-IR spectrum for $\{[Mn(SB^{2+})Re(CN)_7](H_2O)_7\}_n$ **1**.

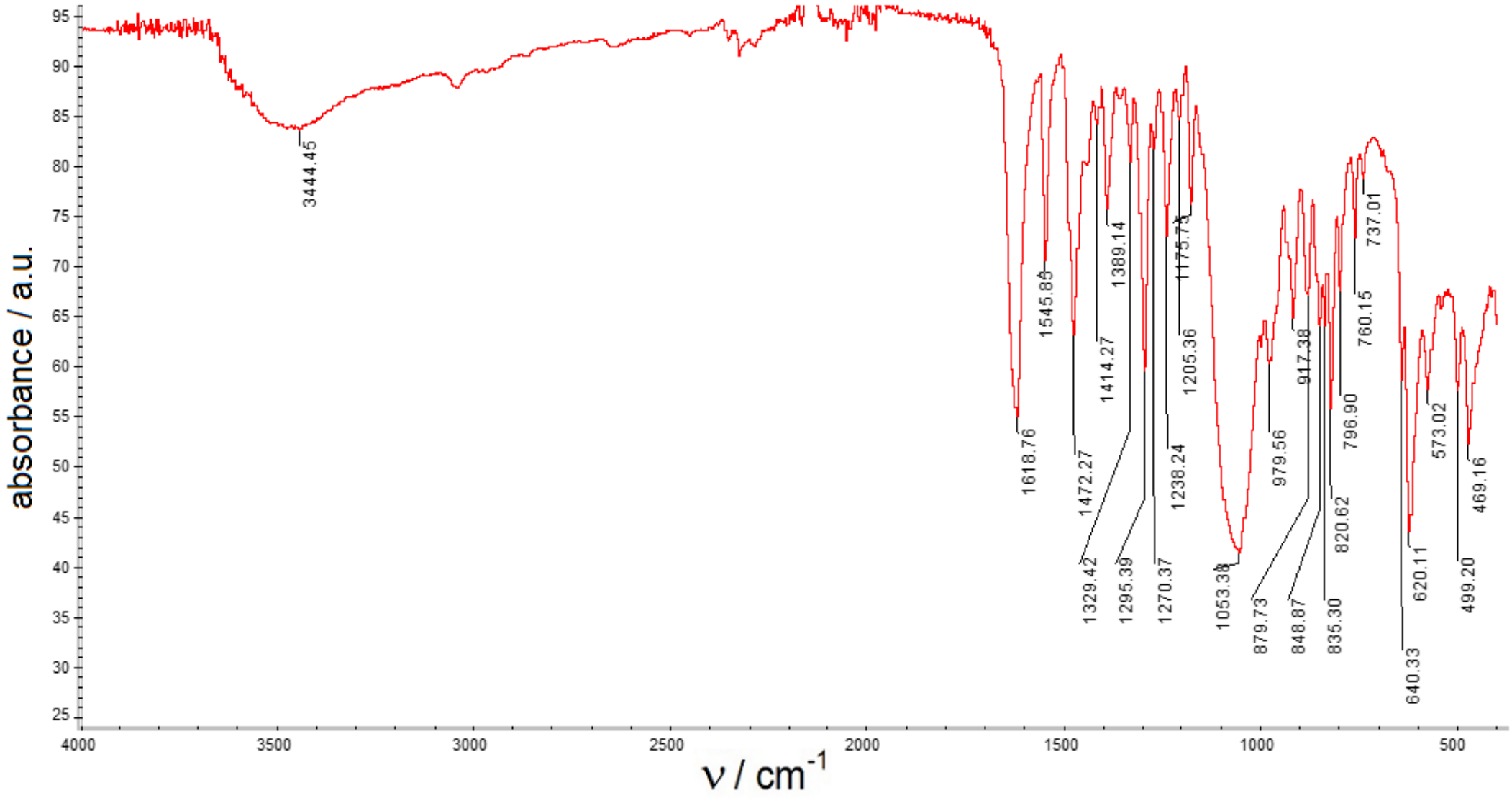

Figure S7. ATR-IR spectrum for the precursor, $[Mn(SB^{2+})(H_2O)_2](ClO_4)_3 \cdot H_2O$.

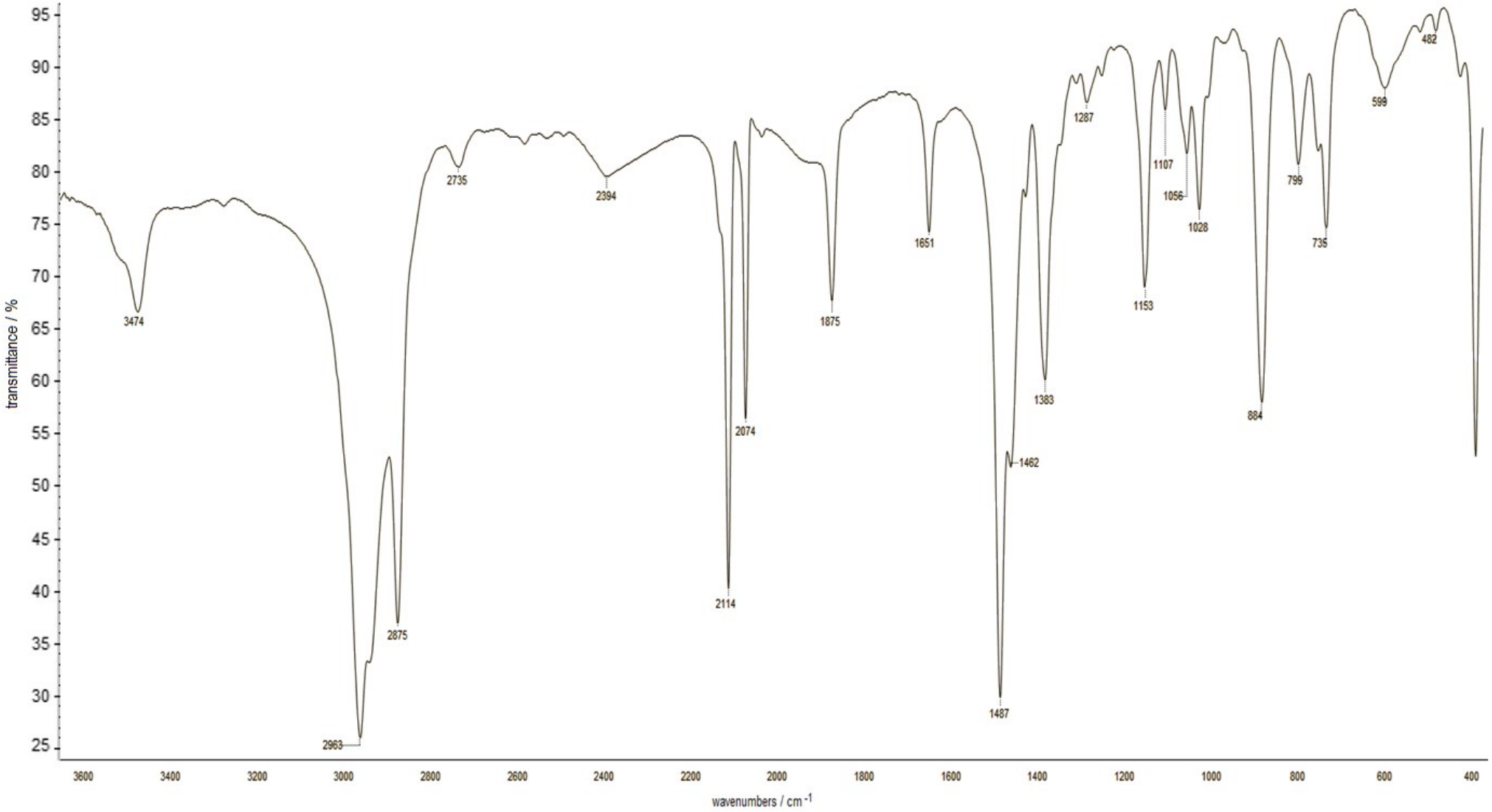

Figure S8. IR spectrum for the precursor, $(Bu_4N)_3[Re(CN)_7]\cdot H_2O$ (KBr).

.

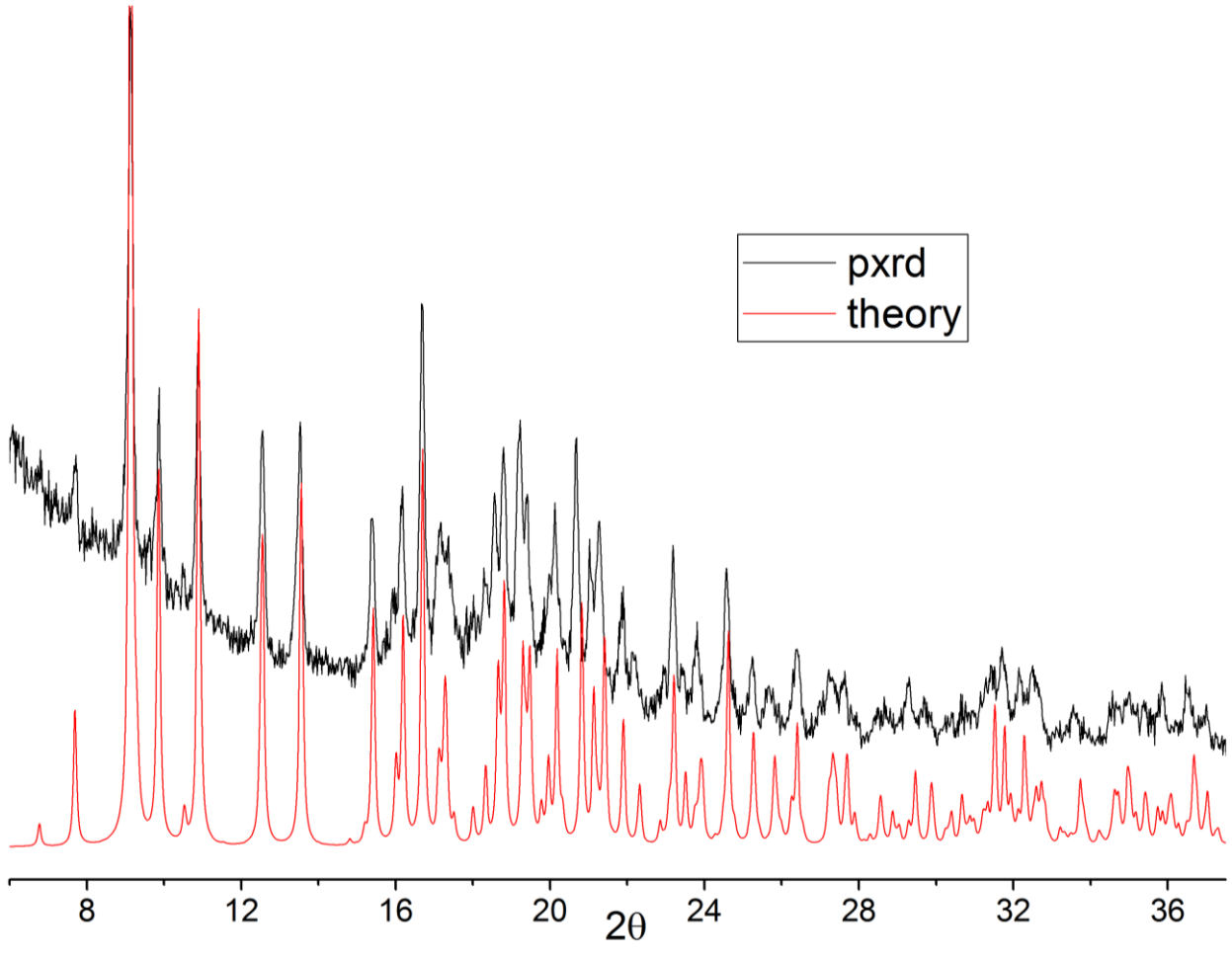

Figure S9. PXRD patterns for the chain compound **1**: polycrystalline sample (black), theoretically calculated (red).

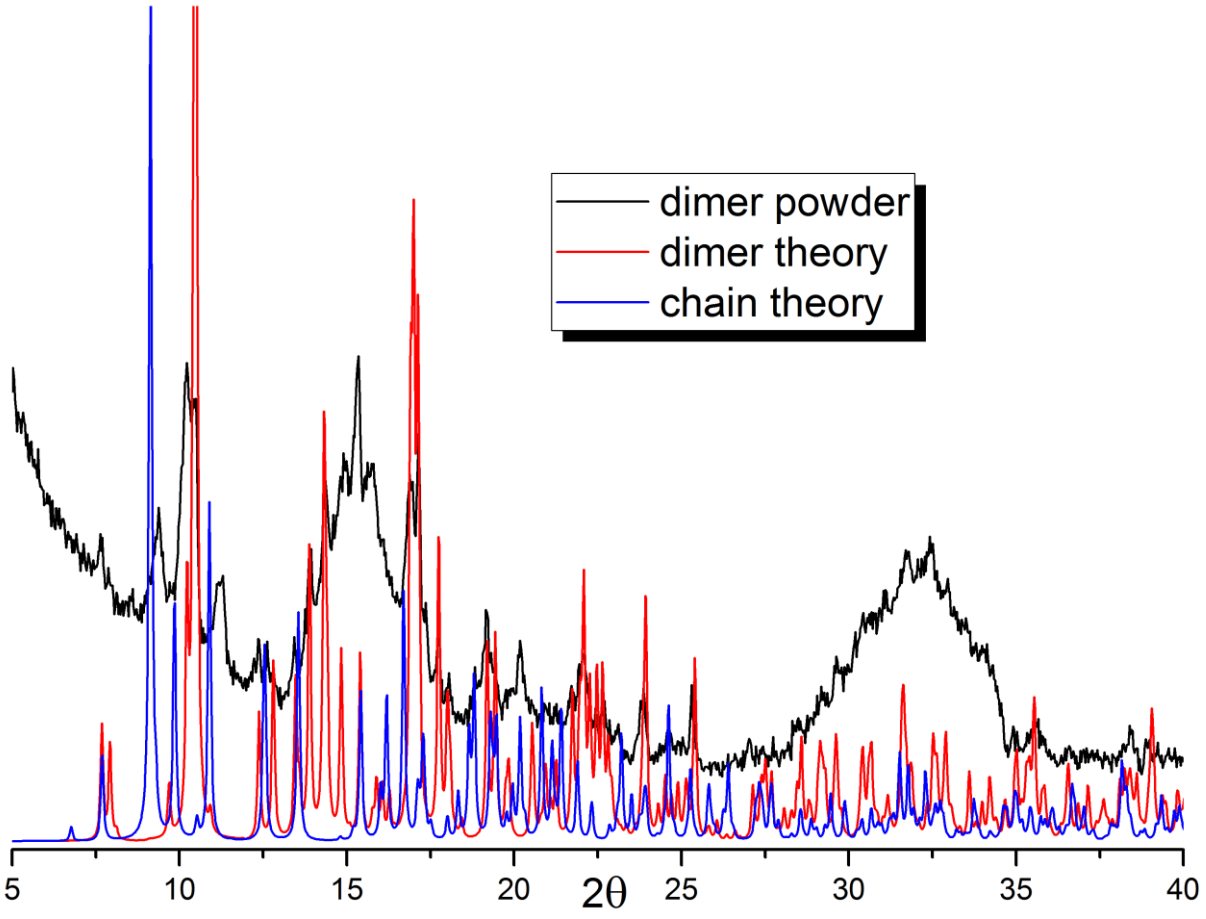

Figure S10. PXRD patterns for the dimer compound **2** (room T) and theoretically calculated (150 K) for **1** and **2**.

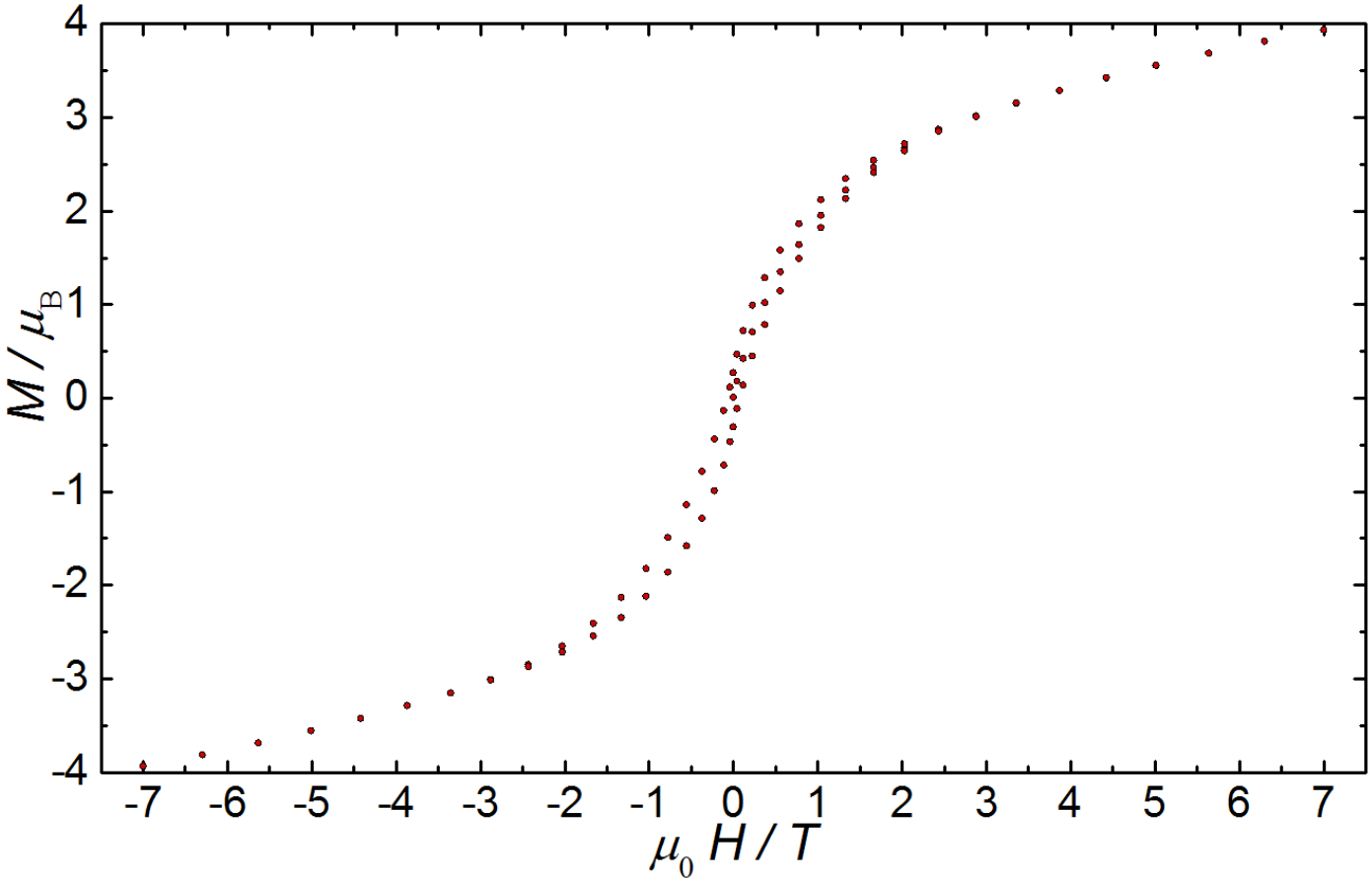

Figure S11. Magnetic hysteresis loop of **2** measured at 1.8 K on a polycrystalline sample (sw. rate – 0.07 $T \cdot s^{-1}$).

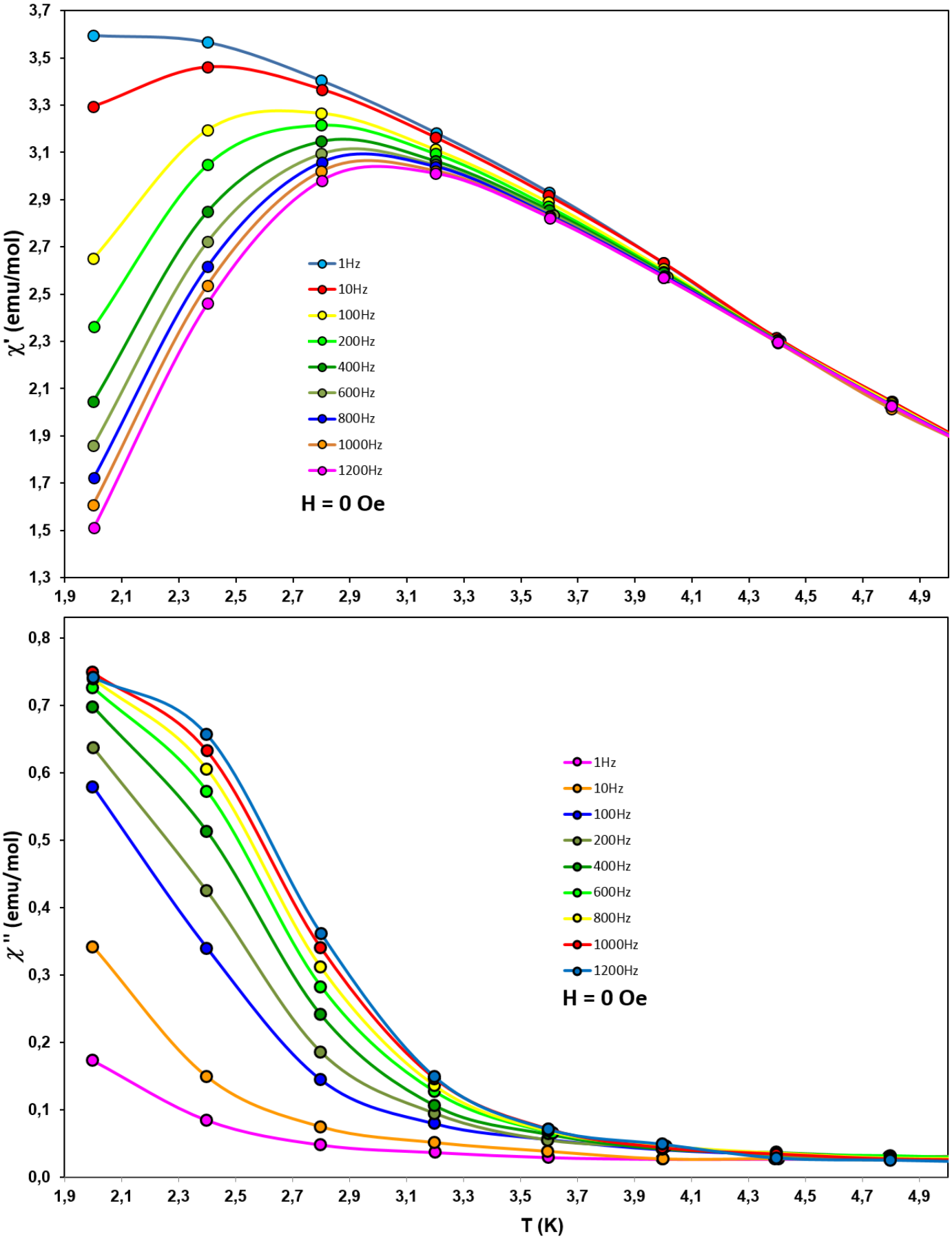

Figure S12. 8. Variable-temperature of the real, χ' (top), and imaginary, χ'' (bottom), parts *ac* molar susceptibility data for **1** under H_{dc} = 0 Oe, H_{ac} = 2.7 Oe. Solid lines are guides.

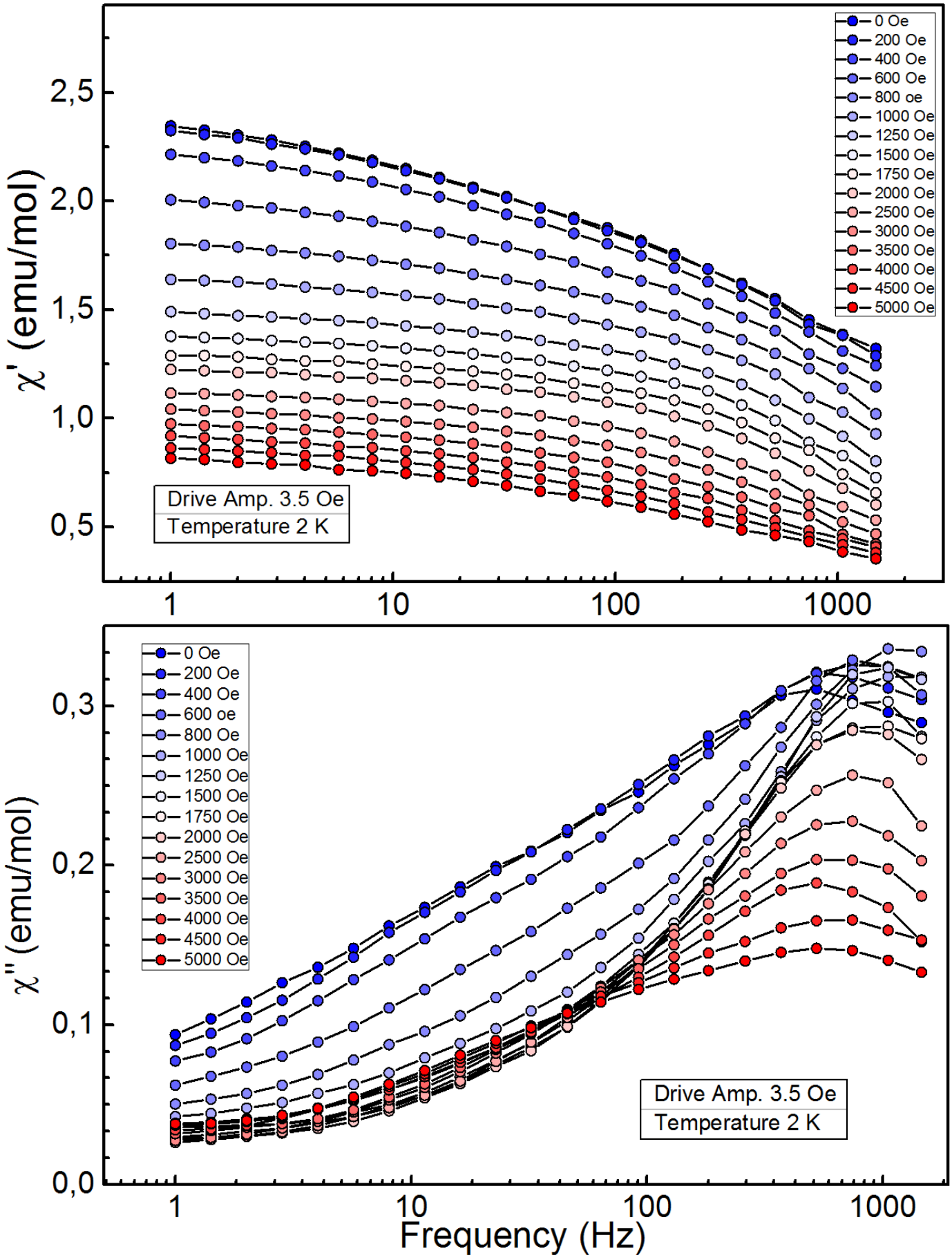

Figure S13. Frequency dependence of the real (χ') (top) and imaginary (χ'') (bottom) parts of the *ac* susceptibility for a polycrystalline sample of **2** in different *dc*-fields y and with applied a 3 Oe *ac* field. Solid lines are guides.

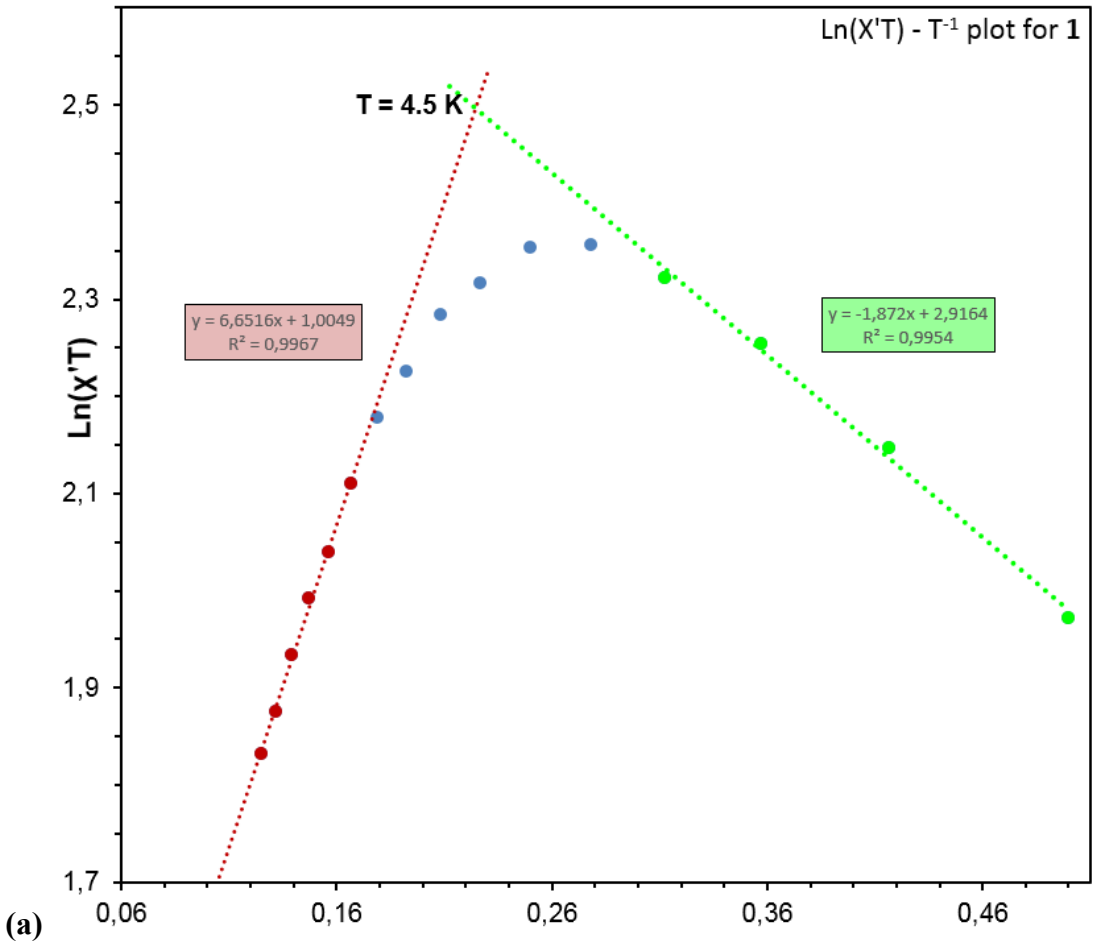

(a)

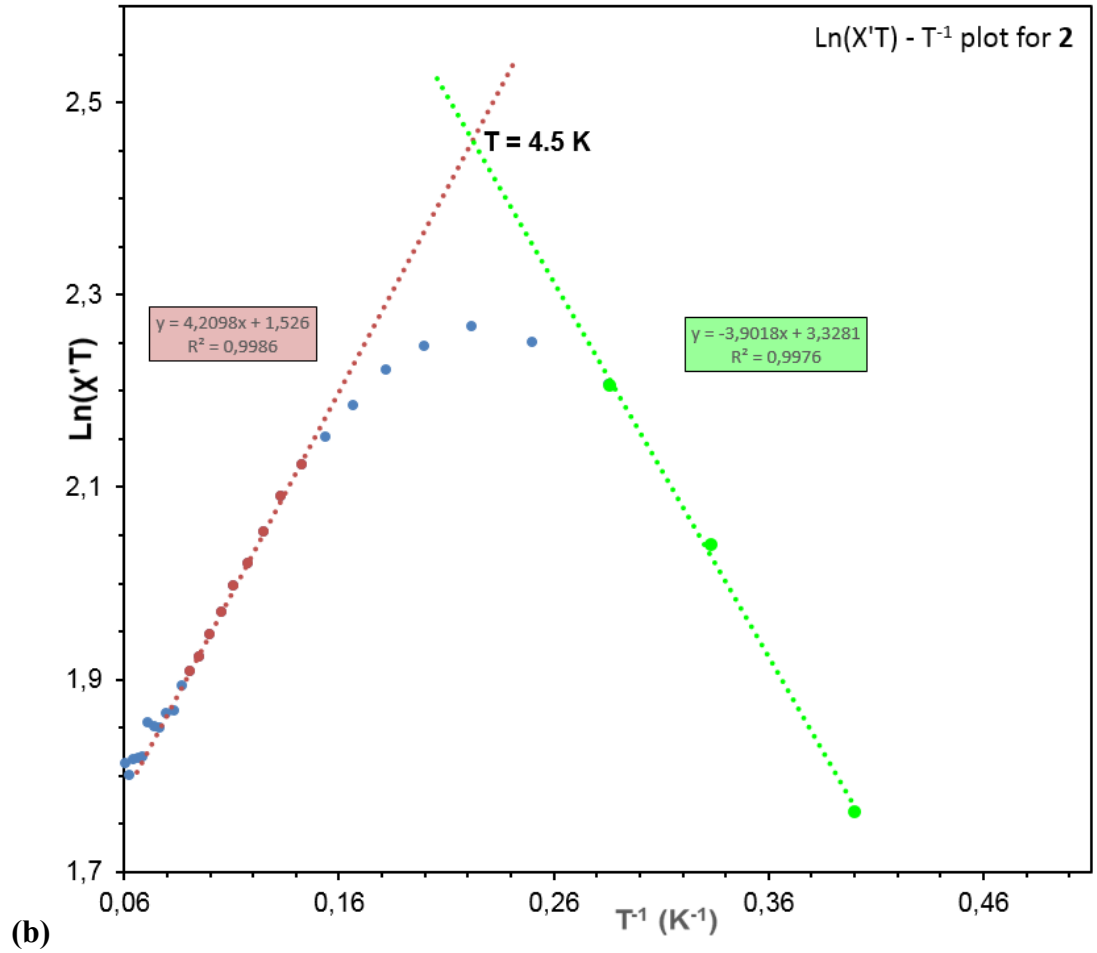

(b)

Figure S14. Plots of ln(X′*T*) vs 1/*T* (where X′ is the molar component of the *ac* susceptibility) for **1** (top) and **2** (bottom) collected in zero applied *dc* field and frequency of 1 Hz. The dashed red lines correspond to a linear fit for high temperature region, giving Δ_ξ/k_B = 6.66 (C_{eff}=1.005 emu·K/mol) and 4.21 K (C_{eff}=1.526 emu·K/mol) for **1** and **2** respectively. The dashed green lines corresponds to a linear fit for low temperature region. An intersection of the two linear regions corresponds to the crossover temperature T^*≈4.5 K equal for both.

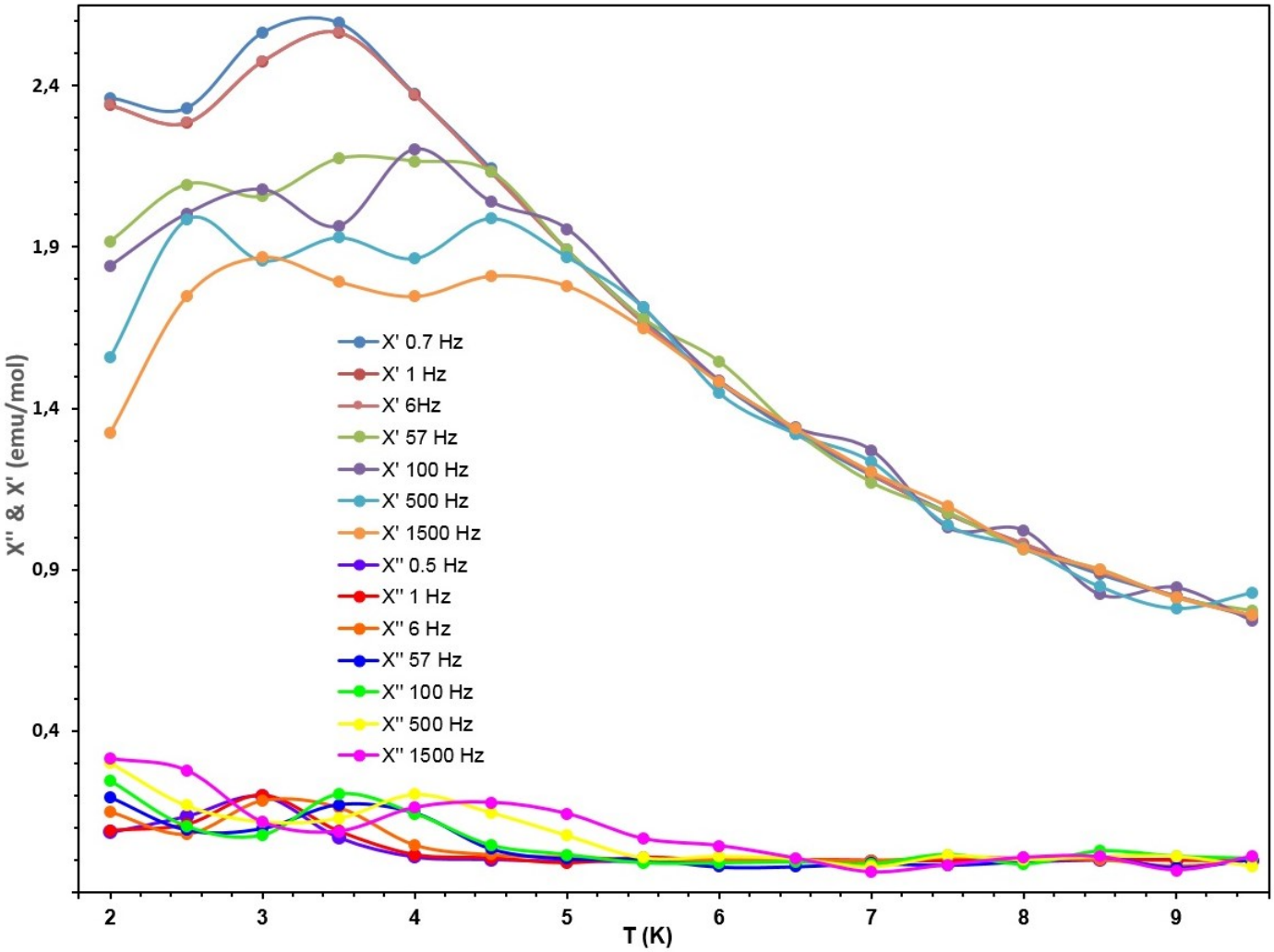

Figure S15. Variable-temperature real, χ' (top) and imaginary, χ'' (bottom) *ac* molar susceptibility data for **2** under H_{dc}=100 Oe, H_{ac}=3.5 Oe. Solid lines are guides.

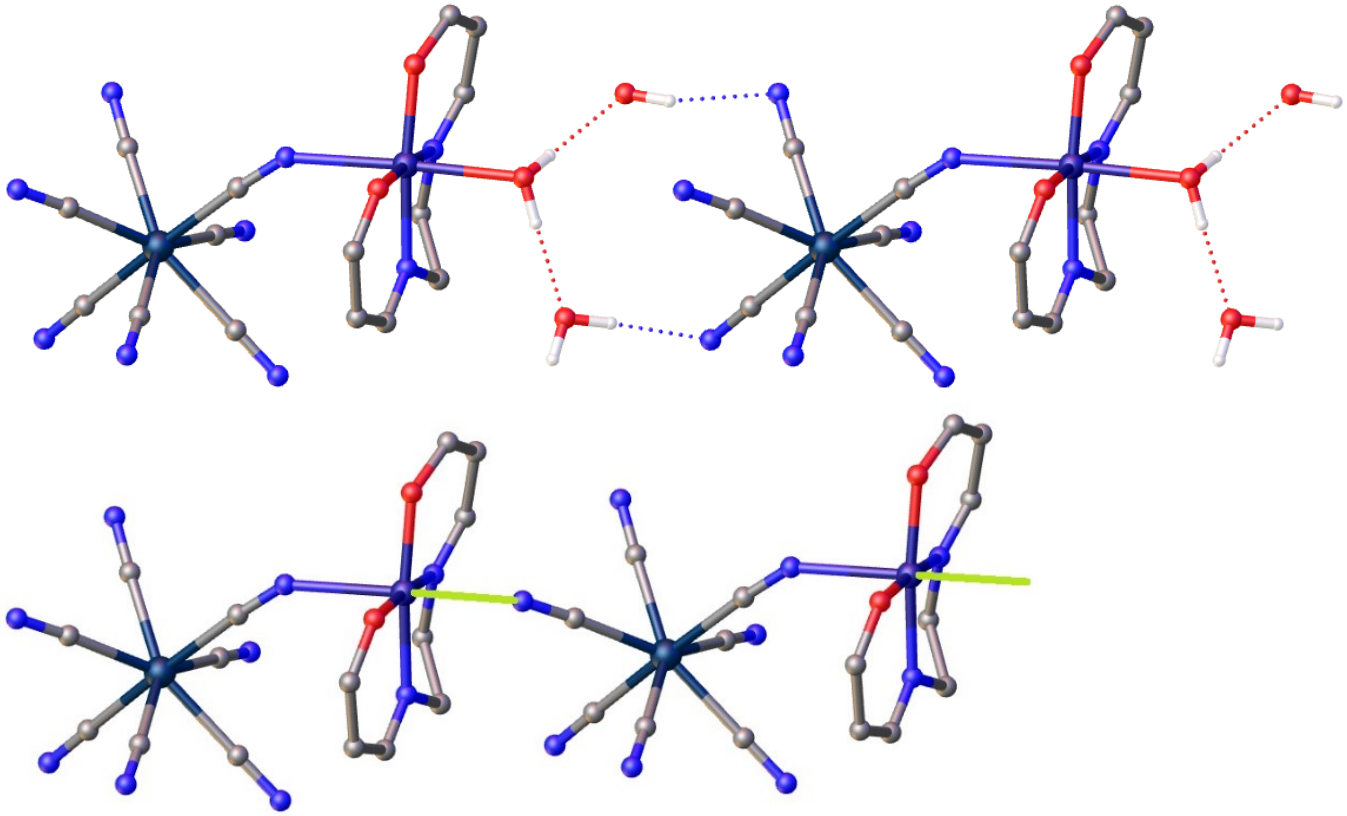

Figure S16. Possible formation of a *1D* polymer from **2** by a desolvation. The $[Mn(SB^{2+})]^{3+}$ complexes are connected to the Re^{IV} ions by an equatorial and an apical cyanide bridges.

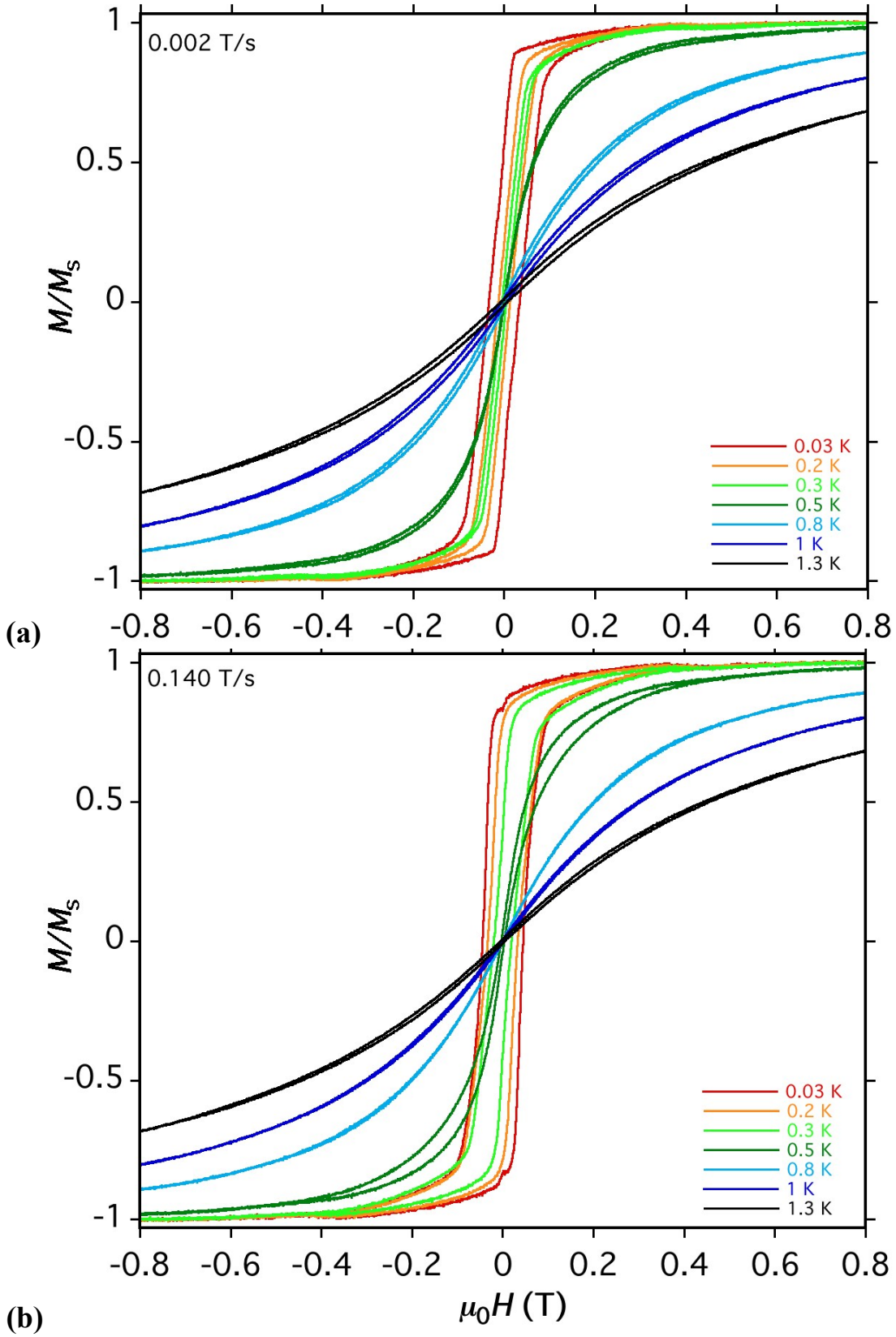

Figure S17. Field dependences of the normalized magnetization at the field sweeping rate of 0.002 $T \cdot s^{-1}$ (a), and 0.140 $T \cdot s^{-1}$ (b), measured at different temperatures on an oriented single crystal of **2** with the magnetic field applied along the easy magnetic axis.

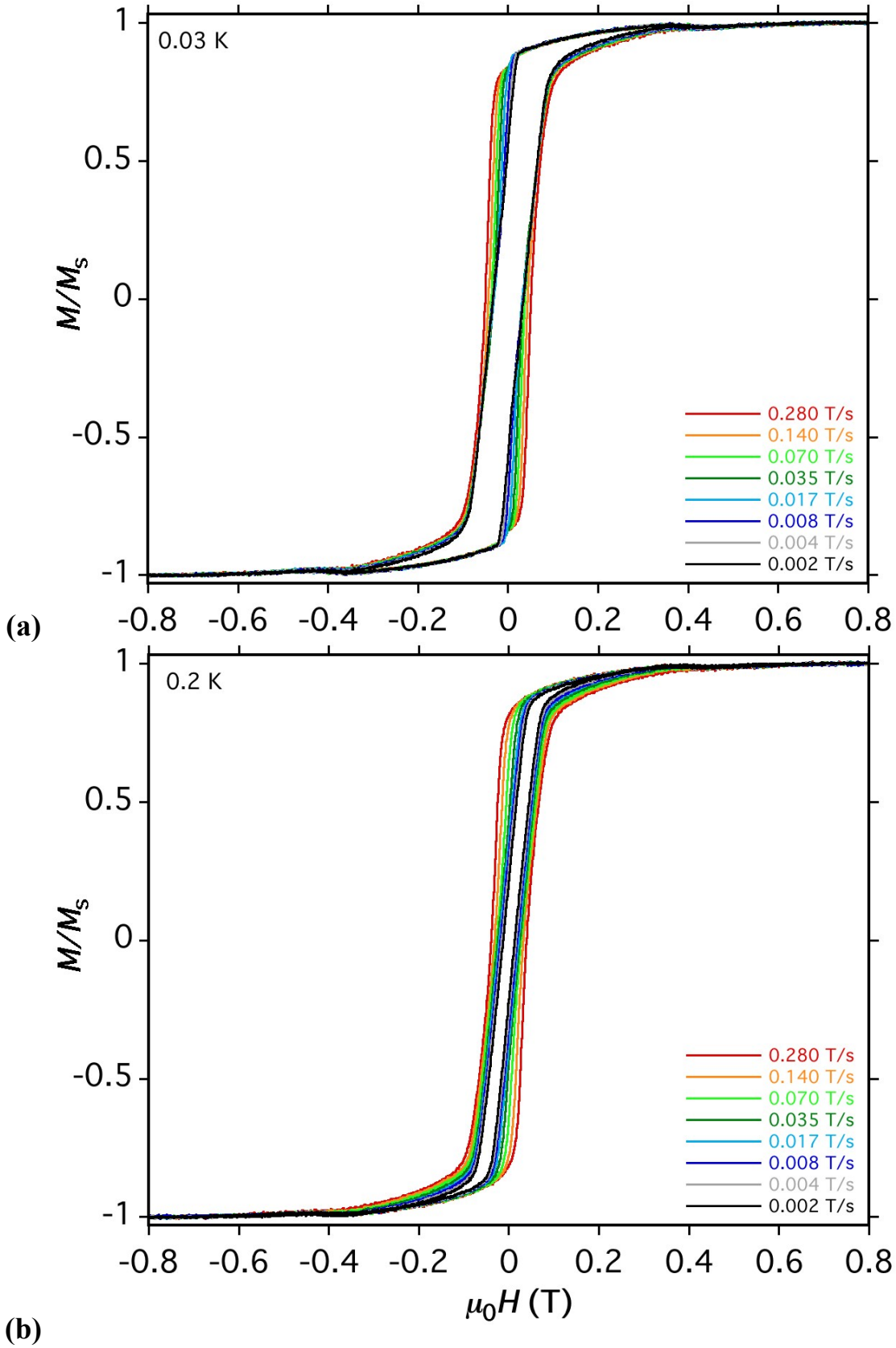

Figure S18. Field dependences of the normalized magnetization at 0.03 K (a), and 0.2 K (b) measured at different field sweeping rates on an oriented single crystal of **2** with the magnetic field applied along the easy magnetic axis. The maximum coercitivity reaches 1043.5 Oe at 30 mK and SwRate of 0.280 $T \cdot s^{-1}$.